Anal. Chem. **2007,** *79,* 930−937

Integrated Refractive Index Optical Ring Resonator Detector for Capillary Electrophoresis

Hongying Zhu,† Ian M. White,† Jonathan D. Suter,† Mohammed Zourob,‡ and Xudong Fan*,†

Department of Biological Engineering, 240D Life Sciences Center, University of Missouri−Columbia, Columbia, Missouri 65211, and Institute of Biotechnology, University of Cambridge, Tennis Court Road, Cambridge CB2 1QT, UK

We developed a novel miniaturized and multiplexed, on-capillary, refractive index (RI) detector using liquid core optical ring resonators (LCORRs) for future development of capillary electrophoresis (CE) devices. The LCORR employs a glass capillary with a diameter of ~100 μm and a wall thickness of a few micrometers. The circular cross section of the capillary forms a ring resonator along which the light circulates in the form of the whispering gallery modes (WGMs). The WGM has an evanescent field extending into the capillary core and responds to the RI change due to the analyte conducted in the capillary, thus permitting label-free measurement. The resonating nature of the WGM enables repetitive light−analyte interaction, significantly enhancing the LCORR sensitivity. This LCORR architecture achieves dual use of the capillary as a sensor head and a CE fluidic channel, allowing for integrated, multiplexed, and noninvasive on-capillary detection at any location along the capillary. In this work, we used electroosmotic flow and glycerol as a model system to demonstrate the fluid transport capability of the LCORRs. In addition, we performed flow speed measurement on the LCORR to demonstrate its flow analysis capability. Finally, using the LCORR's label-free sensing mechanism, we accurately deduced the analyte concentration in real time at a given point on the capillary. A sensitivity of 20 nm/RIU (refractive index units) was observed, leading to an RI detection limit of 10^{-6} RIU. The LCORR marries photonic technology with microfluidics and enables rapid on-capillary sample analysis and flow profile monitoring. The investigation in this regard will open a door to novel high-throughput CE devices and lab-on-a-chip sensors in the future.

Capillary electrophoresis (CE) is a rapid, high-resolution analytical tool and has been used extensively in many chemical and biomedical applications,[1,2] ranging from genome sequencing,[3] proteomics,[4] and clinical and environmental sample analysis[5,6] to chemical cytometry.[7] Detection of CE is typically carried out at the terminal end of the capillary.[1,2] However, in this detection scheme, only the final separated analyte is analyzed, and the detailed information regarding how samples move in the capillary is completely lost.[8,9] To take full advantage of the high resolution and low sample volume achieved by CE, on-capillary detection is highly desirable.[8,9] As compared to end-capillary detection, on-capillary detection can analyze sample separation by providing vital information about the flow profile, such as flow rate and dispersion, while also permitting detection with low sample volume.[10,11] In particular, for CE modes that exhibit self-concentration and self-focusing effects, such as capillary isoelectric focusing, on-capillary detection becomes critical due to its capability of direct monitoring of self-focusing dynamics and fast sample analysis.[12]

On-capillary detection has been accomplished using UV absorption and laser-induced fluorescence (LIF) spectroscopy;[2,8,13,14] however, the sensitivity in UV absorption is generally low due to the short light absorption path and small sample volume. In addition, UV absorption suffers from nonlinear response to sample concentration.[9] Although LIF is the most sensitive detection technique, this method requires the presence of chromophores that are either inherent to the analyte or introduced through labeling. In the former case, intrinsic chromophores may not readily fit the laser lines available in the lab, and their fluorescence is normally weak, leading to the poor signal-to-noise ratio. In the latter situation, labeling processes are laborious and may interfere with the analyte's biochemical functions.

Recently, refractive index (RI) has been used in CE for on-capillary detection[9,11−20] and end-capillary detection,[21] as well as

* To whom correspondence should be addressed. Phone: 573-884-2543. Fax: 573-884-9676. E-mail: fanxud@missouri.edu.
† University of Missouri−Columbia.
‡ University of Cambridge.

(1) Kraly, J.; Fazal, M. A.; Schoenherr, R. M.; Bonn, R.; Harwood, M. M.; Turner, E.; Jones, M.; Dovichi, N. J. *Anal. Chem.* **2006**, *78*, 4097−4110.
(2) Landers, J. P. *Handbook of Capillary Electrophoresis*, 2nd ed.; CRC Press: Boca Raton, 1996.
(3) Dovichi, N. J.; Zhang, J. *Angew. Chem., Int. Ed.* **2000**, *39*, 4463−4468.
(4) Guzman, N. A.; Phillips, T. M. *Anal. Chem.* **2006**, *77*, 60A−67A.
(5) Hu, S.; Dovichi, N. J. *Anal. Chem.* **2002**, *74*, 2833−2850.
(6) Thormann, W.; Lurie, I. S.; McCord, B.; Marti, U.; Cenni, B.; Malik, N. *Electrophoresis* **2001**, *22*, 4216−4243.
(7) Krylow, S. N.; Starke, D. A.; Arriaga, E. A.; Zhang, Z.; Chan, N. W. C.; Palcic, M. M.; Dovichi, N. J. *Anal. Chem.* **2000**, *72*, 872−877.
(8) Bruno, A. E.; Gassmann, E.; Pericles, N.; Anton, K. *Anal. Chem.* **1989**, *61*, 876−883.
(9) Bruno, A. E.; Krattiger, B.; Maystre, F.; Widmer, H. M. *Anal. Chem.* **1991**, *63*, 2689−2697.
(10) Staller, T. D.; Sepaniak, M. J. *Electrophoresis* **1997**, *18*, 2291−2296.
(11) Pawliszyn, J. *Anal. Chem.* **1988**, *60*, 2796−1801.
(12) Wu, X.-Z.; Pawliszyn, J. *Electrophoresis* **2002**, *23*, 542−549.
(13) Schrum, K. F.; Lancaster, J. M., III; Johnston, S. E.; Gilman, S. D. *Anal. Chem.* **2000**, *72*, 4317 − 4321.
(14) Swinney, K.; Bornhop, D. J. *Electrophoresis* **2000**, *21*, 1239−1250.
(15) Bornhop, D. J.; Dovich, N. J. *Anal. Chem.* **1987**, *59*, 1632−1636.
(16) Markov, D.; Dotson, S.; Wood, S.; Bornhop, D. J. *Electrophoresis* **2004**, *25*, 3805−3809.
(17) Wang, Z.; Bornhop, D. J. *Anal. Chem.* **2005**, *77*, 7872−7877.

10.1021/ac061279q CCC: $37.00
Published on Web 12/19/2006

in microchip-based fluidic systems.[22,23] RI detection features a number of advantages in comparison to UV or fluorescence detection. First, it is noninvasive to virtually all analytes; second, it is relatively simple to implement and provides a sensing signal regardless of the existence of absorbing or fluorescent chromophores. As a result, RI detection is considered to be a universally applicable method in microfluidics detection.[14,17,18,23] Moreover, RI detection measures the analyte concentration instead of mass; the detection signal does not scale down with the sample volume, which makes RI detection particularly attractive when ultrasmall (pico-/nanoliter) detection volume is involved.[17,23] RI detection has been implemented in the form of forward scattering,[9,18,23] backscattering,[17] surface plasmon resonance,[21] waveguide,[22] and Fabry−Perot interferometry.[24] Detection limits ranging from 10^{-5} to 10^{-9} RIU have been reported.[2,9,11−24]

Although RI detection has been shown to be a promising technique in CE development, miniaturization and multiplexing of RI detectors have been a challenge.[21] The equipment involved is usually bulky and highly sophisticated, which limits the RI detection to only one or two spots along the capillary. Furthermore, due to relatively large dimensions of the detection spot on the capillary, the resolution in flow spatial profile may be compromised.

In this article, we have developed a novel miniaturized and multiplexed on-capillary RI detection architecture based on liquid core optical ring resonators (LCORRs). The concept of the LCORR is illustrated in Figure 1. The LCORR employs a piece of glass capillary with a diameter of a few tens to a few hundreds of micrometers and a wall thickness of a few micrometers. The circular cross section of the capillary, shown in Figure 1B, forms an optical ring resonator along the capillary. The ring resonator supports the circulating mode of the light, called whispering gallery modes (WGMs),[25] which can be launched by bringing the LCORR into contact with an optical waveguide perpendicular to the LCORR. The capillary wall is sufficiently thin (<4 μm) so that the WGM evanescent field extends beyond the capillary interior surface and detects the analyte in the capillary. Despite the small physical size of the ring resonator, the resonating nature of the WGM enables repetitive light−analyte interaction, thus significantly enhancing the LCORR detection length and sensitivity. The effective detection length L_{eff} can be characterized by the Q-factor of the ring resonator, which determines the number of light circulation cycles supported by the resonator,[25]

$$L_{\text{eff}} = \frac{Q\lambda}{2\pi n} \tag{1}$$

where λ is wavelength and n is the RI of the LCORR ($n = 1.45$). For example, for an LCORR with a Q-factor of 10^6 and λ = 980 nm, L_{eff} can be as long as 10 cm. Such a long detection length is achieved without sacrificing the CE resolution, in contrast to other capillary designs such as "Z-shaped" and "bubble-shaped" capillaries.[2] Moreover, as shown in Figure 1, the LCORR is scalable to a 2-dimensional array, which not only is important for high-throughput CE development, but also allows us to set up a reference channel to reduce thermal induced noise, the biggest limitation in RI detection.[14,17]

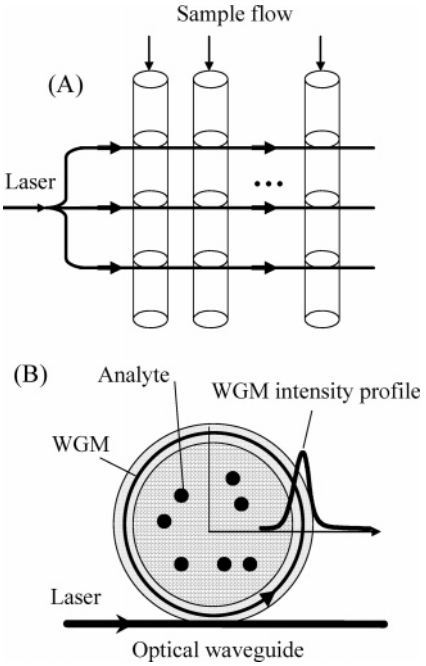

Figure 1. (A) A conceptual illustration of multiplexed on-capillary detection using a 2-dimensional LCORR array. A waveguide array arranged transversely is in contact with the LCORR and launches the WGM. (B) The cross section of an LCORR. The WGM circulates along the LCORR circumference. Its evanescent field extends beyond the interior surface of the LCORR and interacts with the analytes in the core.

The LCORR is unique in that it achieves dual use of the capillary as a sensor head and as a CE fluidic channel. The LCORR belongs to the field of optical ring resonator sensors that has recently been under intensive investigation for bio/chemical detection.[26−35] As discussed in the Theory Section, these sensors utilize RI as the sensing signal; the WGM spectral position shifts in response to the RI change induced by either the bulk solution change near the resonator surface or binding of the analyte to the surface. A detection limit on the order of 10^{-7} RIU and 10^{-6}

(18) Swinney, K.; Markov, D.; Bornhop, D. J. *Analyst.* **1999**, *124*, 221−225.
(19) Krattiger, B; Bruin, G. J. M.; Bruno, A. E. *Anal. Chem.* **1994**, *66*, 1−8.
(20) Deng, Y.; Li, B. *Appl. Opt.* **1998**, *37*, 998−1005.
(21) Whelan, R. J.; Zare, R. N. *Anal. Chem.* **2003**, *75*, 1542−1547.
(22) Lenney, J. P.; Goddard, N. J.; Morey, J. C.; Snook, R. D.; Fielden, P. R. *Sens. Actuators, B* **1997**, *38−39*, 212−217.
(23) Burggraf, N.; Krattiger, B.; de Moller, A. J.; de Rooij, N. F.; Manz, A. *Analyst.* **1998**, *123*, 1443−1447.
(24) Woodruff, S. D.; Yeung, E. S. *Anal. Chem.* **1982**, *54*, 2124−2125.
(25) Chang, R.; Campillo, A. *Optical Processes in Microcavities*; World Scientific Pub Co., Inc.: Singapore, 1996.
(26) White, I. M.; Zhu, H.; Suter, J. D.; Hanumegowda, N. M.; Oveys, H.; Zourob, M.; Fan, X. *IEEE Sens. J.*, in press.
(27) Vollmer, F.; Braun, D.; Libchaber, A.; Khoshsima, M.; Teraoka, I.; Arnold, S. *Appl. Phys. Lett.* **2002**, *80*, 4057−4059.
(28) Vollmer, F.; Arnold, S.; Braun, D.; Teraoka, I.; Libchaber, A. *Biophys. J.* **2003**, *85*, 1974−1979.
(29) Krioukov, E.; Greve, J.; Otto, C. *Sens. Actuators, B* **2003**, *90*, 58−67.
(30) Hanumegowda, N. M.; White, I. M.; Oveys, H.; Fan, X. *Sens. Lett.* **2005**, *3*, 315−319.
(31) White, I. M.; Hanumegowda, N. M.; Fan, X. *Opt. Lett.* **2005**, *30*, 3189−3191.
(32) Zhu, H.; Suter, J. D.; White, I. M.; Fan, X. *Sensors* **2006**, *6*, 785−795.
(33) Hanumegowda, N. M.; White, I. M.; Fan, X. *Sens. Actuators, B* **2006**, *120*, 207−212.
(34) Hanumegowda, N. M.; Stica, C. J.; Patel, B. C.; White, I. M.; Fan, X. *Appl. Phys. Lett.* **2005**, *87*, 201107−1 − 201107−3.
(35) White, I. M.; Oveys, H.; Fan, X. *Opt. Lett.* **2006**, *31*, 1319−1321.

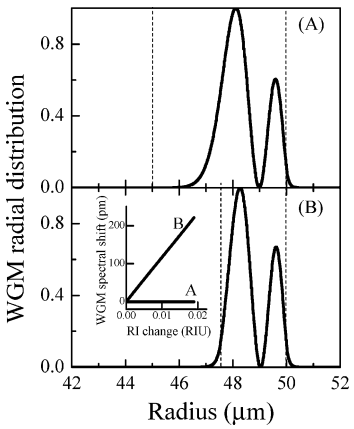

Figure 2. WGM radial distribution for (A) a thick-walled LCORR (o.d./i.d. = 100/90 μm) and (B) a thin-walled LCORR (o.d./i.d. = 100/95 μm). The dashed lines show the interior and exterior surfaces. The structure of the LCORR is water core, $n = 1.333$; glass wall, $n = 1.45$; and surrounding medium, $n = 1.0$. Wavelength = 980 nm. The inset is the theoretically calculated WGM response to the RI change in the core for the thick-walled LCORR (curve A) with a sensitivity of 6×10^{-4} nm/RIU and the thin-walled LCORR (curve B) with a sensitivity of 11 nm/RIU.

RIU has been reported in microsphere-based ring resonator sensors and the LCORR, respectively.[26,34] Moreover, as compared to current capillary technology, the LCORR adds new functionalities of multiplexed on-capillary detection, because the LCORR has ring resonator sensors naturally integrated along the capillary. As shown in Figure 1, the detection light, that is, the WGM, can be launched externally through an array of optical waveguides at any location along the capillary, providing a sensitive, noninvasive, and quantitative tool to monitor the analyte flowing in the core in real time. As shown later, the waveguide lateral size is only a few micrometers; thus, the detection position can be defined along the capillary with a precision down to micrometers, which significantly increases the resolution in determination of the flow profile in the capillary in comparison with state of the art.[2,13,14] Assuming that the LCORR has an inner diameter of 100 μm and a detection window of 10 μm (determined by the extension of the ring resonator along the LCORR), the detection volume for each ring resonator is estimated to be <100 pL.

In this article, we first present the underlying detection theory, followed by a discussion on fabrication and characterization of the LCORR. Then we report on the use of the LCORR with electroosmotic flow (EOF) as a model system to demonstrate its capability for fluid transport, flow analysis, and subsequent quantitative sample analysis. We show that the LCORR is highly compatible with current CE technology and has great potential for development of novel miniaturized high-throughput CE devices.

THEORY

The WGM of the LCORR can fully be described using Mie theory by considering a three-layered radial structure (core, wall, and surrounding medium).[35–37] The radial distribution of the WGM electrical field of an LCORR is governed by

$$E_{m,l}(r) = \begin{cases} AJ_m(k_{m,l}n_1 r) & (r \le r_1) \\ BJ_{\mathrm{m}}(k_{m,l}n_2 r) + CH_m^{(1)}(k_{m,l}n_2 r) & (r_1 \le r \le r_2) \\ DH_m^{(1)}(k_{m,l}n_3 r) & (r \ge r_2) \end{cases} \quad (2)$$

where J_m and $H_m^{(1)}$ are the mth Bessel function and the mth Hankel function of the first kind, respectively. The RI of the core, wall, and the surrounding medium is described by n_1, n_2, and n_3. The terms r_1 and r_2 represent the inner and outer radius of the LCORR, respectively, and $k_{m,l}$ is the amplitude of the wave vector in a vacuum for the lth-order radial WGM. The resonant wavelength $\lambda_{m,l} = (2\pi)/(k_{m,l})$ can be obtained numerically from eq 2 by matching the boundary conditions at r_1 and r_2. Two examples of the electrical field distribution of the WGM are shown in Figure 2.

For the LCORR with the radius much larger than wavelength, the WGM resonance condition can be approximated by a simple expression,[38]

$$\lambda = \frac{2\pi r n_{\mathrm{eff}}}{m} \quad (3)$$

where r is the ring outer radius, and m is an integer number given in eq 2, which represents the angular momentum term. n_{eff} is the effective RI experienced by the WGM and is determined by the RI of the core (sample), capillary wall, and the surrounding medium (e.g., air).[37] Equation 3 shows that resonance occurs for wavelengths when an integer multiple of that wavelength matches the circumference.

The WGM has an evanescent field that extends beyond the dielectric surface and into the core. The bulk solution change near the interior surface or binding of molecules to the interior surface leads to a change in n_{eff}, which in turn changes the WGM resonance condition, as indicated by eq 3. Utilization of the shifts in the WGM spectral position as the sensor signal enables a label-free detection that conveys quantitative and kinetic information about the flow in the core. We have developed an in-house simulation tool based on eq 2 that allows us to simulate the WGM behavior under various experimental conditions, such as wall thickness, LCORR size, and the RI of the core.

To achieve adequate sensitivity, the WGM needs to have sufficient evanescent exposure in the core. Figure 2 compares the WGM radial distribution for a thick-walled (5 μm) and thin-walled (2.5 μm) LCORR of 100-μm o.d. (outer diameter) using Mie theory.[35–37] For the thick-wall case, the amount of the WGM in the core is negligible and the WGM is, thus, insensitive to the RI change in the core. In contrast, when the wall becomes thin, a significant fraction of light is present in the core, resulting in a much higher sensitivity (inset in Figure 2B).

EXPERIMENTAL

Materials. Ethanol, glycerol (99%), sodium phosphate dibasic (Na_2HPO_4, 99%), and hydrofluoric acid (HF, 48%) were purchased from Sigma-Aldrich (St. Louis, MO). Hydrofluoric acid is a particularly dangerous inorganic acid that should be handled with

(36) Bohren, C. F.; Huffman, D. R. *Absorption and Scattering of Light by Small Particles*; John Wiley & Sons, Inc.: New York; 1998.
(37) Suter, J. D.; White, I. M.; Zhu, H.; Fan, X. *Appl. Opt.*, in press.
(38) Knight, J. C.; Dubreuil, N.; Sandoghdar, V.; Hara, J.; Lefevre-Seguin, V.; Raimond, J. M.; Haroche, S. *Opt. Lett.* **1996**, *21*, 698–700.

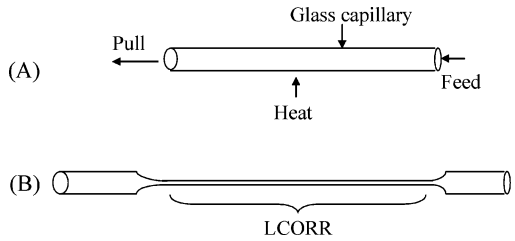

Figure 3. The LCORR fabrication process.

consideration for safety. All chemical agents were used without purification and were prepared in the 18-MΩ water generated by the Easypure-UV system from Barnstead (Dubuque, IA). The glycerol solutions were prepared by initially dissolving the glycerol in 0.001 M Na_2HPO_4 buffer and then further diluting in Na_2HPO_4 to the desired concentrations. Fused-silica and aluminosilicate glass tubes with 1.2-mm o.d. and ~0.9-mm i.d. (inner diameter) were purchased from Sutter Instruments (Novato, CA).

Fabrication and Characterization of the LCORR. Since the thin-walled LCORRs are not readily available commercially, we assembled an in-house pulling station that allowed us to fabricate the LCORRs by rapidly stretching a fused-silica or aluminosilicate glass tube while heating the center section, as illustrated in Figure 3. For a given initial tube size, the final LCORR o.d. is determined by the pulling and feed-in speed, both of which are controlled by a computer. For our experiments, the LCORR o.d. is designed to be in the proximity of 100 μm. The pulling process was terminated immediately when a sufficiently long LCORR was achieved. After systematic investigation in pulling parameters and quality check of the final size and the wall thickness using an optical microscope, we found that the original o.d./i.d. ratio and circularity can well be maintained after pulling. Therefore, the wall thickness of the LCORR thus prepared was approximately 10 μm. With this method, LCORRs of tens of centimeters in length can be made, limited only by the pulling stage's travel distance. For our experiment, by cutting off both ends, only the center portion of the original LCORR was used.

To further reduce the wall thickness to below 4 μm, various concentrations of HF were pumped through the LCORR via a peristaltic pump to slightly etch the LCORR interior wall. This etching process, similar to the one used for fused-silica etching reported in refs 35 and 39, was well-controlled and took 20−60 min. When the desired wall thickness was reached, pure water was pumped through the LCORR to terminate the etching process. Despite the thin wall, the final LCORRs still retain relatively strong mechanical strength and can easily be handled without damage.

Experimental Setup and Detection Schemes. The details of the experimental setup are schematically shown in Figure 4. We used two LCORRs of 115-μm (LCORR no. 1) and 130-μm (LCORR no. 2) o.d. with a length of ~2 cm in the experiment. Each LCORR was connected to two sample reservoirs (9 mm in diameter and 5 mm in height) through UV-curable adhesives. Two hundred volts from a high-voltage source from Spellman (New York, NY) was placed across the LCORR, resulting in an electric field of ~100 V/cm. A digital ammeter from Omega (Stamford, CT) was used to monitor the current passing through the LCORR.

(39) White, I. M.; Hanumegowda, N. M.; Oveys, H.; Fan, X. *Opt. Express* **2005**, *13*, 10754−10759.

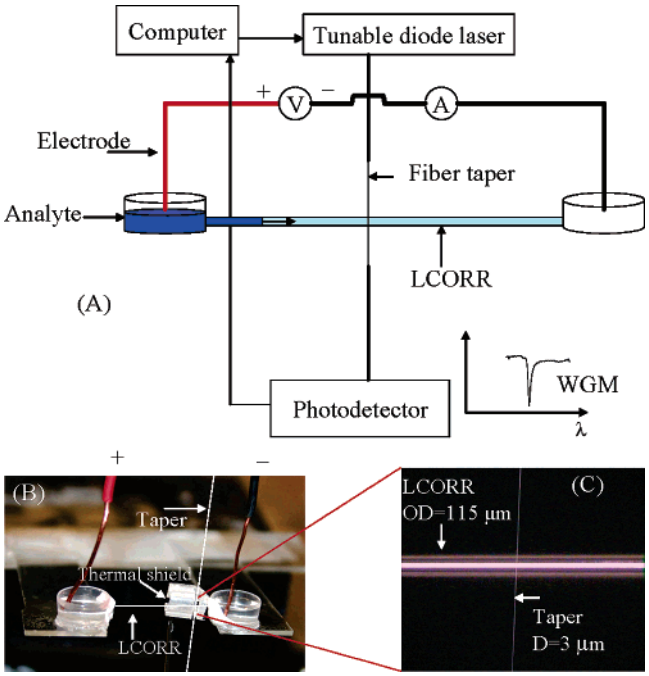

Figure 4. (A) Schematic of EOF experimental setup with a single capillary and a single optical fiber taper. (B) A picture of the experimental setup. A thermal shield is used to reduce the thermal fluctuation caused by air flow. White lines are drawn along the LCORR and the taper to guide the eye. (C) A zoomed-in picture of the LCORR in contact with the taper in the absence of the thermal shield.

An optical fiber taper with a diameter of ~3 μm, fabricated by stretching a single-mode optical fiber under flame,[40] was brought in contact with the LCORR to couple the light from a 980-nm, tunable diode laser from New Focus (San Jose, CA; spectral line width <0.001 pm; repeatability <0.003 pm) into the WGM.

We have developed two approaches to detect the WGM spectral position. In the first approach, a photodetector (no. 1 in Figure 5) was used to monitor the light at the terminal end of the optical fiber, whereas in the second approach, a photodetector (no. 2 in Figure 5) was placed above the LCORR. In both approaches, the laser periodically scanned in wavelength at a constant power. As shown in Figure 5B, when the laser wavelength matches the WGM resonance condition, the light couples into the ring resonator and causes the measured transmission power to drop, leaving a spectral dip at detector no. 1. In the meantime, the light coupled into the LCORR is scattered off the LCORR surface and can be detected as a spectral peak by detector no. 2. Both the measured signals can be used to indicate the WGM spectral position, which shifts in response to the RI change in the LCORR core. The first approach is easy to implement, and the second scheme is more suitable when multiple LCORRs are used for high-throughput LCORR CE development.

In our experiment, since we used only one LCORR as a model system, only detector no. 1 was employed. The laser scanning rate was 5 Hz with a scanning range of 100 pm; the output power was 1−2 mW. The entire measurement system was controlled by a computer through a data acquisition card from National Instruments (Austin, TX). The output power at detector no. 1 for each scan was recorded for post-analysis using in-house spectral

(40) Cai, M.; Vahala, K. *Opt. Lett.* **2000**, *25*, 260−262.

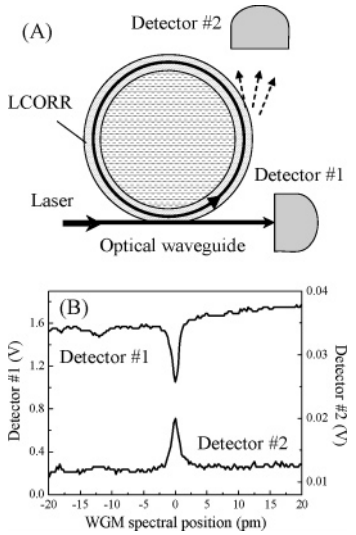

Figure 5. (A) Schemes used for WGM spectral position detection. (B) Transmission signal from detector no. 1 and scattering signal from detector no. 2 indicate the WGM spectral position.

dip detection software. Figure 4B shows a picture of the actual system. Note that a thermal shield was used to reduce the temperature fluctuation induced by air convection. A zoomed-in picture in Figure 4C shows the details of the taper-LCORR system.

RESULTS AND DISCUSSION

Characterization of the LCORR. The LCORR sensor utilizes RI changes in the sample, which are detected by shifts in the WGM resonant wavelength. To perform quantitative detection, the magnitude of the WGM spectral shift must be calibrated to changes in magnitude of the RI, which is the sensitivity curve for the LCORR. We measured this by passing an ethanol−water mixture with well-characterized RI into the LCORR[34,41] while monitoring the resulting WGM spectral shift. To avoid any potential problem in thermally induced WGM shift caused by Joule heat generated by EOF, we connected the LCORR to a peristaltic pump for sample delivery for this characterization. Nevertheless, the detection principle is the same as described in the previous section.

Figure 6 shows the WGM obtained from LCORR no. 2 as an example to demonstrate how to track the WGM response. The line width $\Delta\lambda$ was 0.8 pm, corresponding to a Q-factor of 1.2×10^6 ($Q = \lambda/\delta\lambda$). The WGM shifted to a longer wavelength when the ethanol−water mixture with a higher RI was pumped into the LCORR initially filled with pure water ($n = 1.333$). The WGM of LCORR no. 1 could be tracked in the same manner, and its Q-factor was 2×10^5. As shown in Figure 7A, the sensorgrams for both LCORRs were built by monitoring the evolution of the WGM spectral position when the ethanol was pumped into the LCORR, followed by water rinsing after each ethanol plug. Plotting the RI change versus the respective WGM spectral shift, Figure 7B shows a good linear fit with a sensitivity of 6.6 and 20 nm/RIU for LCORR nos. 1 and 2, respectively. These sensitivities correspond to a wall thickness of 2.8 μm for LCORR no. 1 and 2.3 μm for LCORR no. 2, according to the in-house simulation tool based on Mie theory.[35,37]

(41) Ghoreyshi, A. A.; Farhadpour, F. A.; Soltanieh, M.; Bansal, A. *J. Membr. Sci.* **2003**, *211*, 193−214.

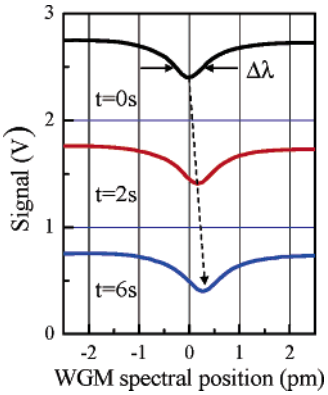

Figure 6. WGM spectral position (from LCORR no. 2) shifted in response to the refractive index change in the LCORR core. Curves for $t = 2$ and 6 s are shifted downward by 1 and 2 V, respectively, for clarity. The Q-factor was 1.2×10^6 and was determined by $\lambda/\Delta\lambda$, where $\Delta\lambda = 0.8$ pm is the full-width-at-half-maximum of the WGM resonance and $\lambda = 980$ nm.

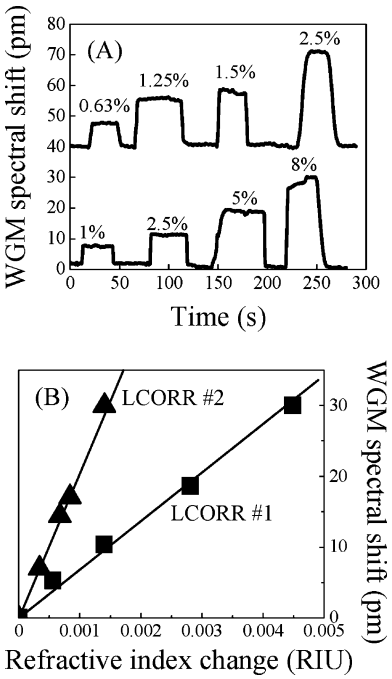

Figure 7. (A) Sensorgrams of the WGM response to various concentrations of ethanol for LCORR nos. 1 (bottom curve) and 2 (top curve). Ethanol concentrations (v/v) are labeled in the figure. Top curve is vertically shifted by 40 pm for clarity. (B) LCORR sensitivity curve obtained with a linear fit of the data in A. Sensitivity is 6.6 and 20.1 nm/RIU for LCORR nos. 1 and 2, respectively.

Glycerol Calibration Curve. Upon establishment of the LCORR sensitivity, we are able to measure the RI calibration curve for glycerol, the analyte used in our experiment. To avoid any potential problem introduced by EOF, we used a peristaltic pump to drive the glycerol of various concentrations into LCORR no. 2. The sensorgram for each concentration was recorded, and the WGM spectral shift was then converted to the RI change using 20 nm/RIU, as plotted in Figure 8.

Demonstration of Electro-osmotic Flow. To demonstrate the flow transport capability of the LCORR, we employed EOF with glycerol as the analyte. EOF plays an important role in capillary electrophoresis, because it is responsible for the bulk fluid transport. Glycerol was chosen, because it is an electrically

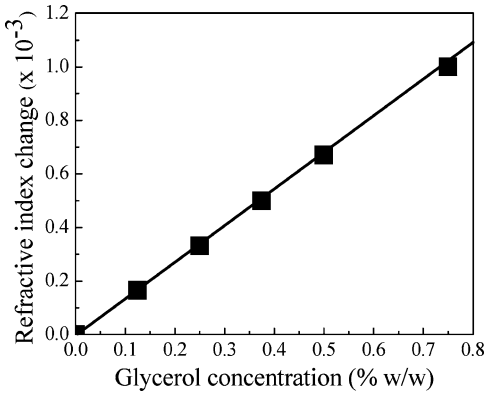

Figure 8. Calibration curve for glycerol. The slope is 0.138 per % w/w.

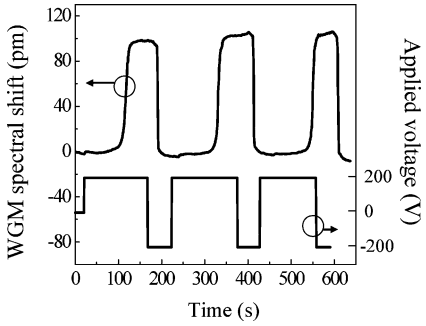

Figure 9. The spectral shift of the WGM of LCORR no. 1 versus time for 7.1% (w/w) glycerol/buffer solution added in the reservoir connected to the positive electrode. The voltage polarity was alternated to drive the glycerol into and out of the LCORR.

neutral marker for EOF flow measurement.[22] Due to HF etching, the LCORR surface is negatively charged; therefore, EOF and glycerol move toward the cathode, which allows us to easily control the analyte flow direction by simply switching the voltage polarity.

In this experiment, LCORR no. 1 was first connected to two reservoirs, as shown in Figure 4. The LCORR and reservoirs were initially filled with 0.001 M Na_2HPO_4 buffer. Then glycerol, premixed with 0.001 M Na_2HPO_4 buffer, was added to the reservoir at the anode. The resulting glycerol concentration in the reservoir was 7.1% (w/w). The liquid in both reservoirs was maintained at the same level to avoid any pressure-driven flow. Figure 9 shows the WGM response to glycerol. The measurement baseline was established in the first 20 s in Figure 9 when the core was filled with buffer. A 200-V power supply was subsequently turned on at $t = 20$ s to drive glycerol toward the cathode. At $t =$ 100 s, an abrupt positive shift was observed in the WGM spectral position, indicating that the glycerol reached the detection spot. The glycerol and buffer reached equilibrium at the ring resonator location 40 s after the onset, as evidenced by the saturation behavior in the WGM shift. Then the polarity of the applied voltage was changed, and 25 s later, the WGM had a negative shift, suggesting that EOF drove glycerol out of the LCORR. The sensorgram moved back to the original level, indicative of complete rinsing. This process was repeated several times.

Flow Analysis with the LCORR. One of the advantages of the LCORR is its capability of performing detection at any location along the capillary. This feature will be very useful in flow analysis, as exemplified in Figure 10, where we carried out flow speed

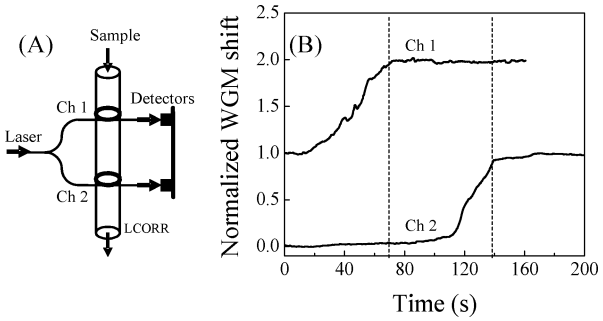

Figure 10. (A) Schematic of flow speed measurement with two channels. (B) Sensorgram from channels 1 and 2. The WGM shift of each channel is normalized to its respective saturation level. The time delay between the two channels was 70 s, as indicated by the dashed lines. Glycerol concentration, 8.3% (w/w); electric field, 90 V/cm; channel spacing, 4.6 mm; flow speed, 0.066 mm/s.

measurement using a two-channel system on LCORR no. 1. Each channel consisted of a ring resonator whose location was defined by the tapers in contact with the LCORR. The channel separation was 4.6 mm. Glycerol was first added to the reservoir, and the electric field of 90 V/cm was subsequently applied across the LCORR at $t = 0$ s. As shown in Figure 10B, at $t = 20$ s, channel 1 started to shift while channel 2 remained virtually unchanged, suggesting that the edge of glycerol flow had reached the ring resonator in channel 1, but had not yet reached channel 2. At $t = 70$ s, channel 1 saturated, indicative of equilibrium between glycerol and buffer solution. The same saturation was reached for the second channel 70 s later. Assuming that the onset of saturation corresponds to the time when the main body of glycerol moves to the ring resonator, we obtain a flow speed of 0.066 mm/s in the LCORR.

In the LCORR, the WGM monitors the flow passing by in real time, and multiple detection positions can be defined at any location; therefore, the LCORR exhibits a large dynamic range in flow rate measurement, as compared to other technologies.[13,16,42,43] Theoretically, there is no upper or lower limit in flow speed measurement. In practice, the highest detectable flow speed is determined by the channel separation and by the laser scanning and data acquisition rate. Under the condition of 1-mm channel separation and 100-Hz scanning rate, which can easily be met, the LCORR can handle a flow rate up to 100 mm/s. Furthermore, the flow rate can be precisely measured due to the high accuracy in detection position determination and the high-speed sampling rate. With higher number of channels involved, the flow rate measurement accuracy can further be improved through averaging.

Thermal Expansion and Thermo-optic Effects. The observed WGM shift could also be caused by thermal expansion and thermo-optic effects resulting from Joule heat in EOF. Thermal expansion changes the LCORR radius, whereas thermo-optic and electro-optic effects change the RI of water (or buffer) and the LCORR wall. All these effects lead to variations in the resonance condition in eq 3.[37] During the experiment, the current through the LCORR was ~2 μA at 200 V for the glycerol concentrations used, resulting in a power of 0.4 mW dissipated

(42) Weimer, W. A.; Dovichi, N. *Appl. Opt.* **1985**, *24*, 2981−2986.
(43) Chen, Z.; Milner, T. E.; Dave, D.; Nelson, J. S. *Opt. Lett.* **1997**, *22*, 64−66.

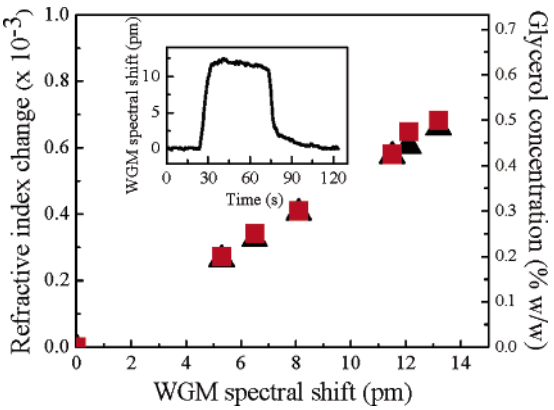

Figure 11. Deduced glycerol concentrations (triangles) in LCORR no. 2 vs actual concentrations in the reservoir (squares). Inset shows the sensorgram when 0.475% (w/w) glycerol was driven into and out of the LCORR by EOF.

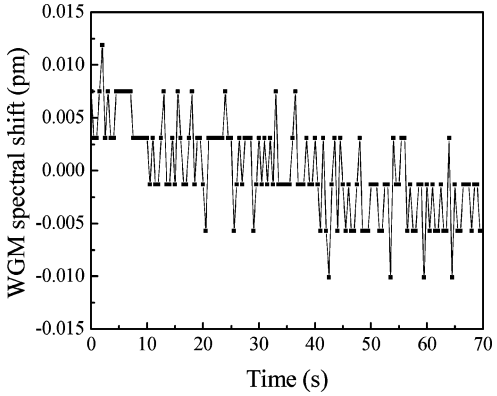

Figure 12. LCORR noise characterization. σ = 0.0065 pm. Wavelength scanning step size = 0.004 pm.

along the entire 2-cm LCORR. It is estimated that the temperature increase was a few tenths of a degree,[9] which, on the basis of a 5−10 pm/K shift rate in an earlier study,[37] corresponds to a WGM shift on the order of 1 pm. Therefore, we conclude that in our experiment, the WGM shifts observed during the glycerol experiment were caused by the RI change due to glycerol.

Quantitative Analysis with the LCORR. In addition to providing a transport mechanism for the sample, the LCORR is capable of on-capillary quantitative sample analysis. To demonstrate this, different concentrations of glycerol were passed through LCORR no. 2 while the WGM spectral position was monitored. First, 200 μL of buffer was added to the cathode reservoir and 150 μL of 0.001 M Na_2HPO_4 buffer was added to the anode. After establishing the baseline, 50 μL of glycerol was injected into the reservoir at the anode. The glycerol mixture was subsequently driven through the LCORR after 200 V was applied, causing the WGM to shift. After each run, the LCORR was cleaned by driving the glycerol completely out of the LCORR, as exemplified in the inset in Figure 11. Then, the reservoirs were cleaned and filled with fresh buffer, and an increased concentration of glycerol was added to repeat the above experiment. During the experiment, the liquid level on the anode side was kept the same as or slightly lower than that on the cathode side to avoid any pressure-driven flow.

Given the observed value of the WGM spectral shift, we can deduce the RI change and, thus, the glycerol concentration in the capillary, as shown in Figure 11. The RI changes were first calculated using the sensitivity of 20 nm/RIU in Figure 7B, and the corresponding glycerol concentrations were then obtained using the glycerol calibration curve in Figure 8. Comparison between the deduced (triangles) and the actual (squares) glycerol concentrations shows a good agreement, attesting to the quantitative analysis capability of the LCORR.

Detection Limit Estimation. Detection limit (DL) of the LCORR can be estimated by

$$\mathrm{DL} = 3\sigma/S \tag{4}$$

where σ is the standard deviation of the system noise in units of pm, which determines the system spectral resolution; S is the LCORR sensitivity in units of nm/RIU; and σ is mainly determined by two factors, that is, the WGM spectral line width and the LCORR thermal noise. For an LCORR with a Q-factor of 10^6 (line width is ~1 pm), 0.01−0.02 pm (1/50 to 1/100 of the line width) can be resolved relatively easily.[44] Thermal noise results in fluctuations in the WGM spectral position through variations in LCORR radius (thermal expansion effect) and in the RI of the wall and the core (thermo-optic effect), as discussed previously. Since water in the core has a negative thermo-optic coefficient, it counteracts the WGM shift due to the thermal expansion and RI change of the wall,[37] in contrast to other RI detection in CE, in which a large thermo-optic effect of water is the dominant noise source.[14,17,23] It has been shown that at a certain wall thickness, the water thermal effect will completely cancel those from thermal expansion and RI changes in the wall, resulting in zero thermal noise.[37] In the LCORR design, we can utilize this phenomenon to our advantage.

In a separate experiment, we characterized the noise level of the LCORR filled with water by placing it on a copper plate on the top of a thermoelectrical cooler from Melcor (Trenton, NJ) controlled by a temperature controller (LDT-5910B, ILX Lightwave, Bozeman, MT). Results plotted in Figure 12 show that σ = 0.0065 pm. Note that this noise includes the noise resulting from data digitization, which is 0.004 pm. Therefore, we believe that the thermal noise may be even smaller. Given S = 20 nm/RIU that has been achieved in LCORR no. 2, the RI detection limit is estimated to be 1×10^{-6} RIU, corresponding to a detection limit of 80 μM for glycerol and other similar chemicals. Considering that protein and DNA molecules typically have a differential RI of 0.2 mL/g,[27,45,46] the detection limit for protein and DNA is estimated to be 5 μg/mL (approximately 100 nM for protein with molecular weight of 50 kiloDaltons and 1 μM for 15-base single-strand oligonucleotides).

CONCLUSIONS AND FUTURE RESEARCH

We have developed a novel on-capillary RI detector based on the LCORR, which integrates the sensitive and noninvasive ring resonator sensors with the capillary. The fluid transport and analysis capability, along with multiple-channel detection, have been demonstrated. The detection limit of 1×10^{-6} RIU was achieved with an LCORR of 2.3-μm wall thickness. The LCORR

(44) Arnold, S.; Khoshsima, M.; Teraoka, I.; Holler, S.; Vollmer, F. *Opt. Lett.* **2003**, *28*, 272−274.
(45) Arakawa, T.; Kita, Y. *Anal. Biochem.* **1999**, *271*, 119−120.
(46) Harrington, R. E. *J. Am. Chem. Soc.* **1970**, *92*, 6957−6964.

system is highly compatible with current CE technology and can further be implemented with integrated optical designs for instrument miniaturization.[47] Moreover, the LCORR is capable of detecting flow at multiple locations, which provides high accuracy in tracking the flow profile in the capillary. In a futuristic design, detection can be performed along the entire capillary so that the sample separation can be monitored en route to the terminal end of a capillary, which will enhance the CE effectiveness in resolution and detection speed.

In addition to conventional CE, the LCORR may also be an excellent platform for immunoaffinity CE (IACE)[4,48] and capillary isoelectric focusing (CIEF).[12] IACE can potentially utilize the LCORR's capability of detecting the binding of the molecules to the interior surface. We recently showed that the detection limit for protein binding is on the order of 10 pg/mm^2.[47,49] For IACE, the inlet of the LCORR will be patterned with different capture molecules for multianalyte detection.[50,51] Thus, the binding and elution processes of analytes, as well as subsequent sample separation, can be monitored using the same LCORR technology. CIEF takes advantage of the high-density, multiplexed, on-capillary detection capability of the LCORR that permits real-time analyte concentration gradient monitoring and fast analyte detection.[12]

Much work has to be done to develop the LCORR into a full-fledged technology. To increase the detection channel density and to integrate and miniaturize the detection system, optical waveguide arrays fabricated with photolithography will be used in replacement of fiber tapers, as has been demonstrated in our recent work.[47] These optical waveguides can be mass-produced with well-defined spacing. High detection channel density in combination with high detection resolution will produce tremendous information regarding the flow in a capillary. Furthermore, a few strategies will be implemented to improve the detection limit. For example, we will introduce a reference channel in the proximity of the detection channel on the same LCORR, which will significantly reduce the common-mode noise.[17,26] Sensitivity will be increased by using an even thinner-walled LCORR, as indicated in Figure 2. Switching the operating wavelength from 980 nm to a longer wavelength, such as 1550 nm, will also enhance the sensitivity. For example, the same LCORR with 2.3-μm-thick wall will yield a sensitivity of 150 nm/RIU when working at 1550 nm, according to our simulation tool based on eq 2. In a longer term, photonic crystal structures using multiple concentric layers coated onto the LCORR will be employed to further expose more light into the core,[52,53] thus increasing the light−analyte interaction. With all these implementations, the detection limit of 1×10^{-7} RIU or lower can be reasonably expected, which makes the LCORR a competitive technology for high-throughput CE development.

(47) White, I. M.; Oveys, H.; Fan, X.; Smith, T. L.; Zhang, J. *Appl. Phys. Lett.* **2006**, *89*, 191106-1−191106-3.
(48) Guzman, N. A. *Anal. Bioanal. Chem.* **2004**, *378*, 37−39.
(49) White, I. M.; Zhu, H.; Suter, J. D.; Oveys, H.; Fan, X. *Proc. SPIE* **2006**, *6380*, 63800F-1 − 63800F-7.
(50) Balakirev, M. Y.; Porte, S.; Vernaz-Gris, M.; Berger, M.; Arie, J.-P.; Fouque, B.; Chatelain, F. *Anal. Chem.* **2005**, *77*, 5474−5479.
(51) Ligler, F. S.; Breimer, M.; Golden, J. P.; Nivens, D. A.; Dodson, J. P.; Green, T. M.; Haders, D. P.; Sadik, O. A. *Anal. Chem.* **2002**, *74*, 713−719.
(52) Xu, Y.; Liang, W.; Yariv, A. *Opt. Lett.* **2003**, *28*, 2144−2146.
(53) Hart, S. D.; Maskaly, G. R.; Temelkuran, B.; Prideaux, P. H.; Joannopoulos, J. D.; Fink, Y. *Science* **2002**, *296*, 510−513.

ACKNOWLEDGMENT

The authors thank the support from a 3M Non-Tenured Faculty Award, the Wallace H. Coulter Foundation, a MU Research Council Award, and a Life Sciences Postdoctoral Fellowship.

Received for review July 14, 2006. Accepted November 9, 2006.

AC061279Q